

Multiple timescale spectral analysis of a linear fractional viscoelastic system under colored excitation

V. Denoël^a,

^a*Structural Engineering Division, Faculty of Applied Sciences, University of Liège, Liège, Belgium*

Abstract

This paper specifies the multiple timescale spectral analysis to the structural analysis of a single degree-of-freedom structure including a fractional derivative constitutive term. Unlike usual existing models for this kind of structure, the excitation is also assumed to be colored, in a low-frequency range compared to that of the structural system, but not necessarily as an integer autoregressive filter. This problem further extends the domain of applicability of the multiple timescale spectral analysis. The solution is developed as a sum of background and resonant components. Because of the specific shape of the frequency response function of a system equipped with a fractional viscoelastic device, the background component is not simply obtained as the variance of the loading divided by the stiffness of the system. On the contrary the resonant component is expressed as a simple extension of the existing formulation for a viscous system, at least at leading order. As a validation case, the proposed solution is shown to recover similar results (in the white noise excitation case) as former studies based on a stochastic averaging approach. A better accuracy is however obtained in case of very small fractional exponent. Another example related to the buffeting analysis of a linear fractional viscoelastic system demonstrates the accuracy of the proposed formulation for colored excitation. This paper is mostly illustrated with the structural analysis of systems equipped with fractional dampers, but it could be re-interpreted in any of the many other fields of engineering where applications are governed by the same equation.

Keywords: Caputo fractional derivative, Riemann-Liouville fractional derivative, perturbation analysis, stochastic averaging, background component, resonant component

1. Introduction

Fractional calculus has attracted considerable attention over the last decades, partly due to the versatility of fractional-order tools to model biological [25, 31], biomedical [22], financial [22] as well as mechanical and structural engineering applications. In mechanics, fractional derivatives are used to model viscoelastic devices [32], whose properties are extracted from dedicated experimental procedures [41]. The stochastic dynamic analysis of systems with fractional viscoelastic devices has been extensively covered, from linear to nonlinear systems and in various cases of stationarity and Gaussianity limitations, and with various type of loadings.

The linearity of the Riemann-Liouville operator [20] makes it rather straightforward to combine viscoelastic devices with others existing features of stochastic dynamics, like frequency dependent parameters [39] or linear systems control theory [8]. It makes it also rather straightforward to generalize the convolution integral [2, 4] or the augmented state formulation [34] to that class of problems. The nonstationary solution of linear systems might also be expressed in closed form [35]. As soon as nonlinear stochastic dynamical systems are considered, the exact solution is usually not obtained in closed form, even for wide-band (usually white noise) excitation. Approximations similar to or derived from the stochastic linearization and stochastic averaging methods [9, 23, 45, 46], or those based on a Fokker-Planck equation of the process envelope [1] appear to be the most classical ways to deal with such problems. Narrow band excitations and complex dynamical interactions can be simplified with similar multiple scales approaches [44]. Other more realistic types of loadings [7] or even earthquake loadings of linear and nonlinear systems equipped with viscoelastic devices have been considered [29, 40].

Beside these approximations of the exact solution of the problem, other numerical techniques have been proposed to deal with the structural analysis of systems with fractional derivatives. In particular, Monte Carlo simulation methods are consistently used to validate approximations. There exist also *ad hoc* simulation methods

Email address: v.denoel@ulg.ac.be (V. Denoël)

30 [35, 11] which are computationally efficient, methods based on Wiener path integral approaches [26, 27, 30, 33]
 31 and weak formulations based on wavelet transforms [28]. These techniques, together with exact assembling
 32 procedures of structural analysis [19], or finite element approaches [3, 17, 18], make it possible to study more
 33 realistic structures composed of several beams and columns, and several viscoelastic devices.

34 This review of the literature reveals two trends. On one side, there are simple dynamical systems with linear
 35 (or linearized) behaviour and white noise excitation, which possess closed form solutions. On the other side,
 36 there are numerical techniques to deal with more realistic loadings (sometimes nonstationary), more realistic
 37 structures and/or slight nonlinearities. The missing gap in-between is related to the understanding (via simple
 38 analytical solutions) of the behavior of complex structures subjected to more realistic loadings. As a first step
 39 towards this goal, we consider the stochastic analysis of a linear system subjected to a low frequency loading
 40 specified by its arbitrary power spectral density. This problem could be studied by means of the usual time
 41 domain multiple scales approach, or the stochastic averaging approach, but would require the consideration of
 42 three interacting timescales as well as fractional models —similar to those used to simulate realizations of wind
 43 fields [12],— for the augmented state coloring the excitation. This seems possible to solve the problem in this
 44 way, although no track evidences of this type of problem has been found in the literature. Instead, we take
 45 advantage of the linearity of the problem to derive a simplified solution in a frequency domain. It is based
 46 on the Multiple Timescale Spectral Analysis [15] which seeks the same objectives as the stochastic averaging,
 47 with slightly more versatility. This method has already been applied in the context of non Gaussian loading
 48 [14], nonstationary loading [6] slightly nonlinear systems [16] or multi degree-of-freedom structures [13, 5]. The
 49 problem considered in this paper is just a little extension of the method and further studies could combine
 50 viscoelastic devices with slight nonlinearities or multiple degrees-of-freedom, for instance.

51 2. Problem Formulation

52 The governing equation of motion of a linear single-degree-of-freedom system equipped with a viscoelastic
 53 device reads

$$m\ddot{y}(t) + g\mathcal{D}^\alpha y(t) + ky(t) = f(t) \quad (1)$$

54 where m is the mass, k is the stiffness, g is the fractional damping coefficient and \mathcal{D}^α is the Riemann–Liouville
 55 fractional derivative operator defined as

$$\mathcal{D}^\alpha y(t) = \frac{1}{\Gamma(1-\alpha)} \int_0^t \frac{\dot{y}(\tilde{t})}{(t-\tilde{t})^\alpha} d\tilde{t}. \quad (2)$$

56 The *fractional exponent* α is assumed to be in the range $[0, 1]$. The two limiting cases correspond to a viscous
 57 damping ($\alpha = 1$) and to a stiffness term ($\alpha = 0$). The stationary external forcing is specified through its power
 58 spectral density function $S_f(\omega)$ and is assumed to vary on a slow timescale, compared to the dynamics of the
 59 structure. This condition is formalized in the sequel. In wind engineering, such a slow loading is typically
 60 attributable to the buffeting loading for which several models exist [38]. For instance, one such model reads

$$S_f\left(\omega; \frac{U}{L}\right) = \sigma_f \frac{0.546 \frac{L}{U}}{\left(1 + 1.64 \frac{L}{U} |\omega|\right)^{5/3}} \quad (3)$$

61 where U and L respectively correspond to the mean wind velocity and the turbulence length scale. The ratio
 62 U/L is a small characteristic frequency that is typical of buffeting excitations [37]. This power spectral density
 63 model is used in the following illustrations. This is just an example; any other low-frequency excitation could
 64 be used to illustrate the following developments.

65
 66 A dimensionless version of the governing equation is obtained by introducing the characteristic time and the
 67 characteristic response

$$t^* = \sqrt{\frac{m}{k}} \quad \text{and} \quad y^* = \frac{\sigma_f}{k} \quad (4)$$

68 and by defining the dimensionless time τ and the scaled response $x(\tau)$ as

$$\tau = \frac{t}{t^*} \quad \text{and} \quad x(\tau) = \frac{y(t^* \tau)}{y^*}. \quad (5)$$

69 Noticing that $\mathcal{D}^\alpha y(t^* \tau) = y^* t^{*\alpha} \mathcal{D}^\alpha x(\tau)$, the governing equation becomes

$$x''(\tau) + 2\xi \mathcal{D}^\alpha x(\tau) + x(\tau) = u(\tau) \quad (6)$$

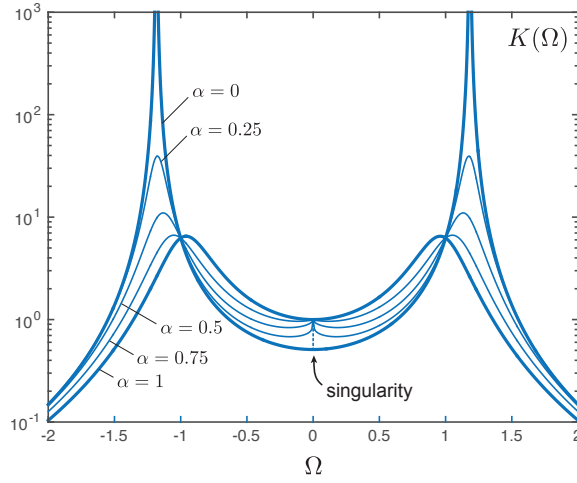


Figure 1: Representation of the kernel $K(\Omega)$ for various values of the fractional exponent α . Other parameters: $\xi = 0.2$,

70 where the prime symbol denotes derivatives with respect to τ , where

$$\xi = \frac{g}{2k t^{\alpha}} = \frac{g}{2m t^{\alpha-2}} \quad (7)$$

71 is the dimensionless *fractional coefficient* and where $u(\tau) = f(\tau t^{\alpha})/\sigma_f$ is the unit-variance dimensionless external
 72 forcing whose power spectral density is given by $S_u(\Omega) = S_f(\Omega/t^{\alpha})/\sigma_f^2 t^{\alpha}$ as a function of the dimensionless
 73 frequency $\Omega = 2\pi/\tau$ (notice that this non-dimensionalization needs to be reviewed in case of white noise
 74 loading, in that case, σ_f can be replaced by $S_f^{1/2}/t^{\alpha}$). The dimensionless version of the power spectral density
 75 of the loading given in (3) reads

$$S_u(\Omega; \beta) = \frac{1}{t^{\alpha}} S_f\left(\frac{\Omega}{t^{\alpha}}; \frac{\beta}{t^{\alpha}}\right) = \frac{0.546}{\beta \left(1 + 1.64 \frac{|\Omega|}{\beta}\right)^{5/3}} \quad (8)$$

76 with $\beta = Ut^{\alpha}/L \ll 1$ the dimensionless characteristic frequency of the turbulence velocity. Again, we repeat
 77 this is just an example and any other loading characterized by power spectral densities whose frequency content
 78 is centered on a small frequency β would perfectly fit the scope of this paper.

79 The Fourier transform of (6) reads

$$(1 + 2\xi\mathcal{C}|\Omega|^{\alpha} - \Omega^2 - 2\xi i\mathcal{S}|\Omega|^{\alpha}) X(\Omega) = U(\Omega) \quad (9)$$

80 where $\mathcal{C} = \cos \frac{\alpha\pi}{2}$ and $\mathcal{S} = \sin \frac{\alpha\pi}{2}$, so that the power spectral density of the response is given by

$$S_x(\Omega) = \frac{S_u(\Omega)}{(1 + 2\xi\mathcal{C}|\Omega|^{\alpha} - \Omega^2)^2 + (2\xi\mathcal{S}|\Omega|^{\alpha})^2} := K(\Omega)S_u(\Omega). \quad (10)$$

81 In this expression, we have defined the kernel (frequency response function) $K(\Omega)$ of this problem. It is illustrated
 82 in Figure 1 for several values of α . It has some peculiarities: (i) the resonance peak located near $\Omega = \pm 1$ in the
 83 viscous case ($\alpha = 1$) regularly moves to higher frequencies as $\alpha \rightarrow 0$, i.e. as the fractional derivative term tends
 84 to correspond to a stiffness term. In the limiting case $\alpha = 0$, the fractional derivative corresponds to a usual
 85 stiffness term and the peak is located at abscissa $\Omega_p = \sqrt{1 + 2\xi} \simeq 1 + \xi$; (ii) the frequency response function
 86 passes through a common *crossing point*, at abscissa $\Omega = 1$, no matter the fractional exponent α (this is readily
 87 observed by replacing Ω by 1 in the definition of the kernel); (iii) in the range $\Omega \in [-1; 1]$ the kernel is comprised
 88 in the area generated by the two limiting cases $\alpha = \{0, 1\}$ with $\alpha = 0$ being the lower bound and $\alpha = 1$ being
 89 the upper bound; (iv) the coordinate at the origin is $K(0) = 1$ provided $\alpha \neq 0$. As $\alpha \rightarrow 0$, a short boundary
 90 layer, whose extent is of order α , develops in the neighborhood of the origin and creates the transition from the
 91 upper bound $K(0) = 1$ to the lower bound $K(\Omega) \simeq \frac{1}{(1+2\xi)^2}$. For $\alpha \rightarrow 0$, the size of this transition zone tends to
 92 zero; for $\alpha = 0$, there is no transition anymore and $K(0) = \frac{1}{(1+2\xi)^2}$.

93 As a result of the fractional powers of Ω appearing in $K(\Omega)$, the response of the system, its variance, defined
 94 as

$$\sigma_x^2 = \int_{-\infty}^{+\infty} S_x(\Omega) d\Omega, \quad (11)$$

95 is unfortunately not available in a simple closed form, even for simple forms of the power spectral density of
 96 $u(\tau)$.

97 In the sequel we assume that $\xi \ll 1$. This is very similar to the developments based on stochastic averaging,
 98 van der Pol transformations, quasi-Hamiltonian systems and the likes and results in three timescales in the
 99 problem : (i) the slow timescale of the loading β^{-1} , (ii) the slow timescale associated with the energy of the
 100 system ξ^{-1} and (iii) the fast (unit) timescale associated with the phase of the system. Unlike existing approaches
 101 exploiting the smallness of ξ in the time domain, we also recognize the existence of the different scales and exploit
 102 it, but in the frequency domain. As shown next, this allows a very simple derivation of the approximate solution
 103 of the problem. The method is based on the Multiple Timescale Spectral Analysis, which is briefly summarized
 104 before tackling the problem at hand.

105 3. Multiple Timescale Spectral Analysis

106 The multiple timescale spectral analysis is a general framework developed to derive approximate responses of
 107 stochastic systems involving various well separated timescales [15]. In this paper, we only need the steady-state
 108 1-D version of the method, which is summarized as follows. Let us consider a (linear, for the sake of this study;
 109 but it could be slightly nonlinear) structural system subjected to a stationary stochastic input. The steady-state
 110 variance of the response is given by

$$\sigma_x^2 = \int_{-\infty}^{+\infty} K(\Omega) S_u(\Omega) d\Omega. \quad (12)$$

111 Instead of the numerical computation of this integral, one might be interested in an approximate closed form
 112 expression, by taking advantage of the timescale separation. To do so, the multiple timescale spectral analysis
 113 consists first in identifying all different contributions to the integral. They might be either global, i.e. on a
 114 domain of order 1 or more, or local in which case they look like a peak over a short domain. The existence
 115 of one or several small numbers in the problem might be used to justify the distinctness of the peaks and is
 116 useful to estimate the order of magnitude of each contribution. In a second step, these contributions to the
 117 integral are evaluated, in a sequential manner, starting with the domain or peak that contributes the most to
 118 the integral. This evaluation develops in several steps: (i) provide a local approximation $\hat{K}(\Omega)\hat{S}_u(\Omega)$ of the
 119 integrand $K(\Omega)S_u(\Omega)$ that is accurate over the considered domain or peak, and that drops to zero in the far
 120 field, in order to be integrable (this condition is very similar to the management of Poincaré's secular terms in
 121 the time domain version of the multiple timescale method). This approximation should also be simple enough
 122 so that the integral

$$\sigma_{x,1}^2 = \int_{-\infty}^{+\infty} \hat{K}(\Omega)\hat{S}_u(\Omega) d\Omega \quad (13)$$

123 corresponding to the first contribution might be evaluated in an explicit way; (ii) once this is done, subtract
 124 (13) from (12), in order to obtain a remainder $r_1 = \sigma_x^2 - \sigma_{x,1}^2$ which is evaluated as the integral of $K(\Omega)S_u(\Omega) -$
 125 $\hat{K}(\Omega)\hat{S}_u(\Omega)$. This integrand does not have any significant contribution anymore, in the neighborhood of the
 126 peak(s) that has/have already been treated. The sequence then follows with the next contribution. When the
 127 process is over, the last remainder is neglected. It provides the order of magnitude of the error committed with
 128 the approximation. Please refer to [15] for more details and examples.

129 4. Solution of the problem and discussion

130 Figure 2 shows some examples of the power spectral density of the structural response given by (10). This
 131 function features two distinct types of peaks: one in the low-frequency range around $\Omega \simeq 0$ and over a domain
 132 whose extent is of order β (the background component) and the other in the order-one frequency range (the
 133 resonant component). We successively focus on these two types peaks in the sequel. They are well distinct
 134 because $\beta \ll 1$.

135 4.1. Background component

136 Following the general method of the multiple timescale spectral analysis, we first focus on the background
 137 component, in the low-frequency range, and define a local approximation of $S_x(\Omega)$. Similarly to what is done
 138 for the oscillator with viscous damping [15], only $K(\Omega)$ is approximated. The stretched coordinate ζ , defined as

$$\Omega = \beta\zeta \quad \Longleftrightarrow \quad \zeta = \frac{\Omega}{\beta}$$

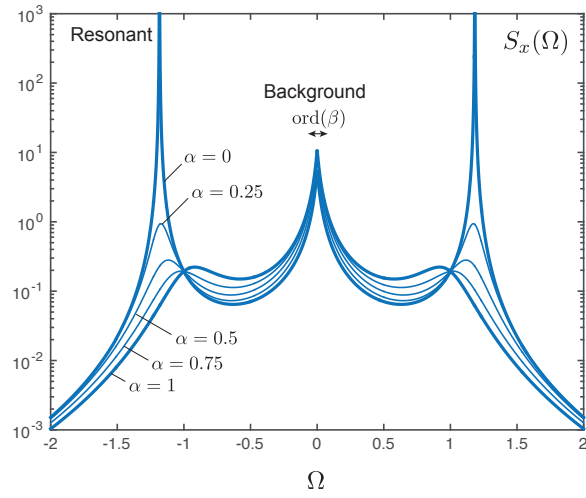


Figure 2: Examples of the power spectral density of the structural response for various values of the fractional exponent α . Other parameters: $\xi = 0.2$, $\beta = 0.05$.

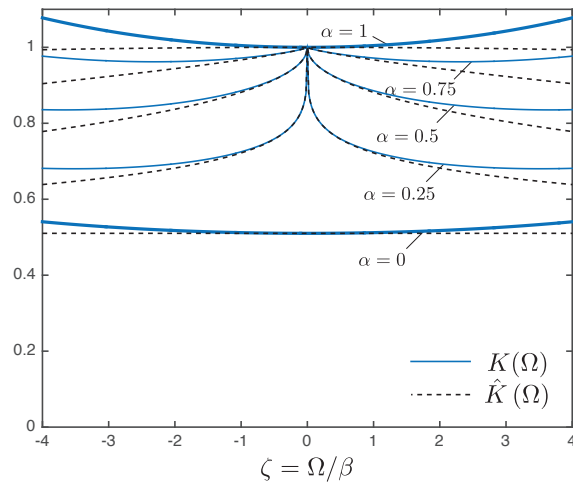


Figure 3: Local approximation of the kernel in the neighborhood of the origin, represented for various values of the fractional exponent α . Illustration given for $\xi = 0.2$.

139 is introduced in order to rescale the range $\Omega = \text{ord}(\beta)$ to an order-one interval when $\zeta = \text{ord}(1)$. Using this
 140 scaling, the kernel is expressed as

$$K[\Omega(\zeta)] = \frac{1}{(1 + 2\xi\mathcal{C}\beta^\alpha |\zeta|^\alpha - \beta^2\zeta^2)^2 + (2\xi\beta^\alpha\mathcal{S} |\zeta|^\alpha)^2}. \quad (14)$$

141 An approximation of this exact kernel is necessary to establish a closed-form expression of the background
 142 component. Evoking the smallness of $\beta \ll 1$, while the stretched coordinate ζ is of order 1, we can drop the
 143 term $\beta^2\zeta^2$ in the first term of the denominator and approximate the exact kernel by

$$\hat{K}[\Omega(\zeta)] = \frac{1}{1 + 4\xi\mathcal{C}\beta^\alpha |\zeta|^\alpha + 4\xi^2\beta^{2\alpha} |\zeta|^{2\alpha}}. \quad (15)$$

144 This is the frequency response function of a lowpass fractional filter [42]. This approximation is represented in
 145 Figure 3, for several values of α . This figure also shows $K[\Omega(\zeta)]$ for $\alpha = 0$ and shows that the singular behavior
 146 at $\zeta = 0$ is well captured. A Taylor series expansion for β around 0 would certainly not have provided such an
 147 accurate approximation. Expression (15) fits the requirements of the multiple timescale spectral analysis since
 148 it is seen to be locally accurate even when $\alpha = 0$; furthermore it is bounded in the far field and has a more
 149 or less simple analytical expression. Using this approximation, the background component of the response is
 150 finally expressed as

$$\sigma_{x,b}^2 = \int_{-\infty}^{+\infty} S_u(\Omega) \hat{K}(\Omega) d\Omega = \int_{-\infty}^{+\infty} \frac{S_u(\Omega)}{1 + 4\xi\mathcal{C} |\Omega|^\alpha + 4\xi^2 |\Omega|^{2\alpha}} d\Omega. \quad (16)$$

151 For $\alpha \simeq 1$ and $\xi \ll 1$, this dimensionless background component is a small perturbation of 1 as a result of
 152 our choices for the scaling of the problem. The integral in (16) requires numerical integration as soon as $\alpha \neq 1$.
 153 We notice however that this integral only depends on the loading parameters ξ and α and is independent of the
 154 properties of the dynamical system. This integral could therefore be determined once and for all, for a given
 155 loading $S_u(\omega)$.

156 Nevertheless there are two alternative solutions to avoid the numerical computation of this integral. First,
 157 the kernel might be approximated as $\tilde{K}(\Omega) \simeq 1$ and the background component could be approximated as

$$\tilde{\sigma}_{x,b}^2 = \int_{-\infty}^{+\infty} S_u(\Omega) d\Omega = 1. \quad (17)$$

158 This approximation is much simpler, consistent with viscous damping [15] but does not capture the rapid
 159 decrease of the kernel for $\alpha \ll 1$ in the neighborhood of the origin. This is further discussed next.

160 Instead, driven by the fact that we would like to recover $\hat{K}[\Omega(\zeta)] \simeq (1 + 2\xi)^{-2}$ in the limit case $\alpha = 0$,
 161 we could determine a Padé approximant (a rational fraction approximation in ξ) by redefining $\hat{K}[\Omega(\zeta)]$ as
 162 $(1 + 2\xi)^{-2}$ multiplied by the series expansion of $(1 + 2\xi)^2 \hat{K}[\Omega(\zeta)]$. For consistency, this series is truncated after
 163 the second term. After some developments, this results in the new approximation

$$\bar{K}(\Omega) = \frac{1 + 4\xi(1 - \mathcal{C} |\Omega|^\alpha) + 4\xi^2(1 - 4\mathcal{C} |\Omega|^\alpha - (1 - 4\mathcal{C}^2) |\Omega|^{2\alpha})}{(1 + 2\xi)^2} \quad (18)$$

164 which yields

$$\bar{\sigma}_{x,b}^2 = \int_{-\infty}^{+\infty} S_u(\Omega) \bar{K}(\Omega) d\Omega = 1 - \frac{4\xi\mathcal{C}(1 + 4\xi)}{(1 + 2\xi)^2} m_{u,\alpha} - \frac{4\xi^2(1 - 4\mathcal{C}^2)}{(1 + 2\xi)^2} m_{u,2\alpha} \quad (19)$$

165 where $m_{u,\alpha} = \int_{-\infty}^{+\infty} S_u(\Omega) |\Omega|^\alpha d\Omega$ is the α -fractional spectral moment of $S_u(\Omega)$. Depending on the high-
 166 frequency behavior of the external forcing, its α - and 2α -fractional spectral moments might not be defined.
 167 In case one of them (or even $m_{u,0} = 1$, the first term in the expression) is unbounded, they should not be
 168 included in the expression of the background component. This other approximation is interesting but has limited
 169 applicability for this reason.

170 In the following section, we continue the derivation with the more accurate expression $\sigma_{x,b}^2$.

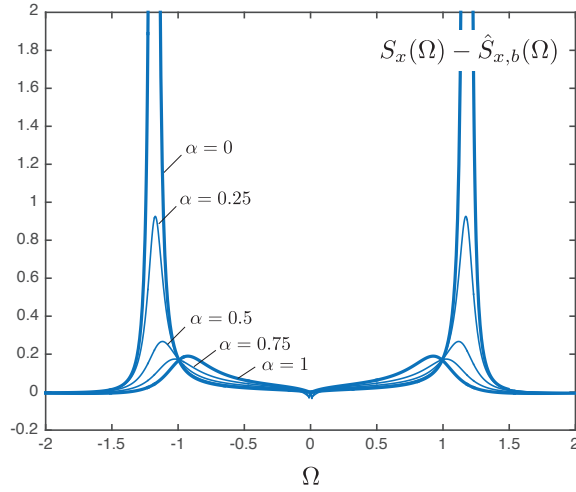


Figure 4: Remainder after subtraction of the background component, represented for various values of the fractional exponent α . Other parameters: $\xi = 0.2$, $\beta = 0.05$.

171 4.2. Resonant component

172 The remainder is obtained by subtracting this first approximation from the original function to integrate,
173 that is

$$r_1 = \int_{-\infty}^{+\infty} S_x(\Omega) - S_u(\Omega)\hat{K}(\Omega) d\Omega = \int_{-\infty}^{+\infty} S_u(\Omega) \left(K(\Omega) - \hat{K}(\Omega) \right) d\Omega. \quad (20)$$

174 The function to be integrated features two symmetrical peaks which will equally contribute the resonant part
175 of the response. They first need to be accurately localized, at least in terms of orders of magnitude. In a second
176 step, the local approximation will be derived.

177 Assuming that the power spectral density of the loading varies smoothly in the neighborhood of the peaks
178 of the frequency response function of the system (located at $\pm\Omega_p$), the peaks in the response are located at the
179 same abscissa as the peaks in the kernel. The actual position of these peaks is then obtained by canceling the
180 first derivative of the denominator of the kernel $K(\Omega)$. It is therefore given by

$$\Omega_p \left(1 + 2\xi\mathcal{C} |\Omega_p|^\alpha - \Omega_p^2 \right) \left(\alpha\xi\mathcal{C} |\Omega_p|^{\alpha-2} - 1 \right) + 2\alpha\xi^2\mathcal{S}^2 |\Omega_p|^{2\alpha-1} = 0. \quad (21)$$

181 Unfortunately, because of the fractional derivatives, this expression does not accept any explicit solution. In-
182 stead, we take advantage of the smallness of ξ and use the first iteration of an iterative scheme [21] to obtain
183 an approximation of the root. Initializing the iterative scheme with $\Omega_{(1)} = 1$, defining the iterative scheme by

$$\Omega_{(k)} \left(1 + 2\xi\mathcal{C} |\Omega_{(k)}|^\alpha - \Omega_{(k+1)}^2 \right) \left(\alpha\xi\mathcal{C} |\Omega_{(k)}|^{\alpha-2} - 1 \right) + 2\alpha\xi^2\mathcal{S}^2 |\Omega_{(k)}|^{2\alpha-1} = 0 \quad (22)$$

184 and retaining the positive root, we obtain an explicit solution for $\Omega_{(2)}$

$$\Omega_{(2)} = \left(1 + 2\xi\mathcal{C} + \frac{2\alpha\xi^2\mathcal{S}^2}{\alpha\xi\mathcal{C} - 1} \right)^{1/2}. \quad (23)$$

185 The Mac Laurin series expansion of that solution for ξ yields an explicit approximation of the position of the
186 peak $\Omega_p \simeq \Omega_{(2)}$ that reads

$$\Omega_p = 1 + \mathcal{C}\xi - \left[\alpha + \left(\frac{1}{2} - \alpha \right) \mathcal{C}^2 \right] \xi^2 + \mathcal{O}(\xi^2). \quad (24)$$

187 The position of the peak is a perturbation of 1 (again, as a result of the scaling). The peak located in \mathbb{R}^- is
188 symmetrically located. For $\alpha \simeq 1$, the fractional derivative resembles a viscous effect, $\mathcal{C} = \cos \frac{\alpha\pi}{2} \ll 1$ and the
189 position of the peak is very close to $1 - \xi^2$, the peak of the viscously damped system. For $\alpha \simeq 0$, $\mathcal{C} \simeq 1$ and the
190 position of the peak is located close to abscissa $1 + \xi$; this is consistent with what has been announced earlier.
191 This is also consistent with existing results obtained with a stochastic averaging approach, at least at leading
192 order in ξ [46].

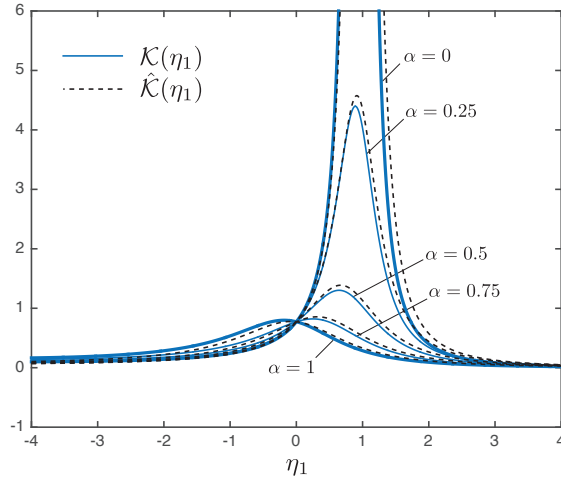


Figure 5: Remainder after subtraction of the background component, represented for various values of the fractional exponent α . Other parameters: $\xi = 0.2$, $\beta = 0.05$.

193 Now that the position of the peak is determined, we can introduce a stretched coordinate η to focus on the
 194 resonant contribution to the response. It is expected that the more accurate the localization of the peak, the
 195 more accurate the final solution. However, to make the solution more accurate has a certain cost and it might
 196 not be optimal to keep a second-order accurate solution in ξ . In this paper we will develop two solutions in
 197 parallel: in the first one, we assume that the position of the peak is located at $\Omega_p = 1$ while, in the second, we
 198 assume that the position of the peak is located at $\Omega_p = 1 + \mathcal{C}\xi$, which is more accurate but results in longer
 199 expressions, at least during the developments.

200 In the first case, the stretched coordinate η_1 is naturally chosen as

$$\Omega = 1 + \xi\eta_1 \iff \eta_1 = \frac{\Omega - 1}{\xi}$$

201 while in the latter, it is chosen as

$$\Omega = 1 + \mathcal{C}\xi + \xi\eta_2 \iff \eta_2 = \frac{\Omega - 1 - \mathcal{C}\xi}{\xi}.$$

202 With the first stretching, the factor in the parenthesis in (20) becomes after some simplifications

$$\mathcal{K}(\eta_1) := \frac{1}{4\xi^2} \frac{1}{\eta_1^2(1 + \frac{1}{2}\eta_1\xi)^2 + (1 + \eta_1\xi)^{2\alpha} - \mathcal{C}\eta_1(2 + \xi\eta_1)(1 + \xi\eta_1)^\alpha} - \hat{K}[\Omega(\eta_1)]. \quad (25)$$

203 No matter the chosen approximation for the background component ($\sigma_{x,b}^2$ or $\tilde{\sigma}_{x,b}^2$), the last term might be
 204 dropped since it is composed of terms which are two to three orders of magnitude smaller than the first term.
 205 Further considering that $\eta_1\xi \ll 1$, we can derive an approximation for the new kernel that reads

$$\hat{\mathcal{K}}(\eta_1) := \frac{1}{4\xi^2} \frac{1}{\eta_1^2 - 2\mathcal{C}\eta_1 + 1}. \quad (26)$$

206 Notice that we could easily get rid of the fractional powers. This approximation is simple, locally accurate (for
 207 $\eta_1 = \text{ord}(1)$) and bounded in the far field. Figure 5 shows a comparison of the exact integrand $\mathcal{K}(\eta_1)$ in the
 208 remainder and this first approximation. The corresponding approximation of the remainder is

$$\hat{r}_1 = \int_{-\infty}^{+\infty} S_u[\Omega(\eta_1)] \hat{\mathcal{K}}(\eta_1) \xi d\eta_1 \quad (27)$$

209 which is further simplified by assuming that $S_u[\Omega(\eta_1)]$ does not vary significantly in the neighborhood of
 210 $\eta_1 = \text{ord}(1)$, which yields

$$\hat{r}_1 = S_u(1) \int_{-\infty}^{+\infty} \hat{\mathcal{K}}(\eta_1) \xi d\eta_1 = \frac{S_u(1)}{4\mathcal{S}\xi} \left[\arctan \left(\frac{\eta_1 + 1}{\eta_1 - 1} \tan \frac{\alpha\pi}{4} \right) \right]_{-\infty}^{+\infty} = \frac{\pi S_u(1)}{4\mathcal{S}\xi}. \quad (28)$$

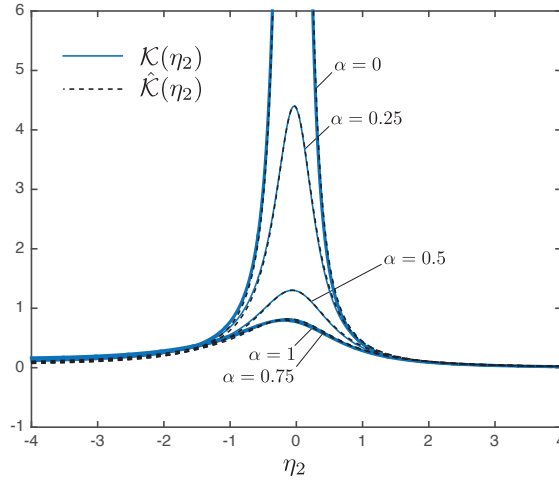


Figure 6: Remainder after subtraction of the background component, represented for various values of the fractional exponent α . Other parameters: $\xi = 0.2$, $\beta = 0.05$.

211 The resonant component of the response is then obtained by multiplying this approximation by 2, in order to
 212 account for the two symmetrical peaks,

$$\tilde{\sigma}_{x,r}^2 = \frac{\pi S_u(1)}{2S\xi}. \quad (29)$$

213 For $\alpha \simeq 1$, the fractional derivative term in the governing equation resembles a viscous damping, $S \simeq 1$, and
 214 the resonant term corresponds to the well-known response of a linear viscous oscillator subject to white noise
 215 excitation [36]. For $\alpha \simeq 0$, the fractional derivative term resembles a stiffness term, in which case the considered
 216 problem tends to an undamped oscillator which is known to have no steady state solution and requires being
 217 studied with other approaches [10, 43]. The approximation in (29) is therefore very simple and compact and
 218 recovers some well-known limiting cases. As anticipated before, it might however be inaccurate when $\alpha \rightarrow 0$
 219 since the location of the peak might be too different from 1, which was the assumption to derive this first
 220 solution.

221 Using the second stretching, the factor in the parenthesis in (20) becomes after dropping the last term (for
 222 same reason as before),

$$\mathcal{K}(\eta_2) := \frac{1}{4\xi^2 [\mathcal{C}(1 + \mathcal{C}\xi + \xi\eta_2)^\alpha - (1 + \frac{1}{2}\mathcal{C}\xi + \frac{1}{2}\xi\eta_2)(\mathcal{C} + \eta_2)]^2 + 4\xi^2 S^2 (1 + \mathcal{C}\xi + \xi\eta_2)^{2\alpha}}. \quad (30)$$

223 Expanding the square and using the binomial theorem stating that $(1 + \epsilon)^\alpha = 1 + \alpha\epsilon + \text{ord}(\epsilon^2)$,

$$\mathcal{K}(\eta_2) = \frac{1}{4\xi^2} \frac{1}{(1 + \frac{1}{2}\mathcal{C}\xi + \frac{1}{2}\xi\eta_2)^2 (\mathcal{C} + \eta_2)^2 - 2\mathcal{C}(1 + \alpha\mathcal{C}\xi + \alpha\xi\eta_2)(1 + \frac{1}{2}\mathcal{C}\xi + \frac{1}{2}\xi\eta_2)(\mathcal{C} + \eta_2) + (1 + 2\alpha\mathcal{C}\xi + 2\alpha\xi\eta_2)}. \quad (31)$$

224 This expression of the kernel is still a little too long and might require further simplification. The denominator
 225 of $\mathcal{K}(\eta_2)$ is a fourth order polynomial in η_2 , which yields four poles in the complex plane and the two peaks
 226 located at $\Omega = \pm\Omega_p$ on the real axis. A much better job is done by focusing on one peak at a time. To do so, we
 227 are free to drop the degree of the polynomial from 4 to 2, by discarding all terms of the denominator involving
 228 third and fourth powers of η_2 , and making sure only one peak on the real axis remains. This approach is similar
 229 to what was done with the first stretching when simplifying (25) into (26); it is also deeply discussed in [15].

230 After a bit of standard algebra and some simplifications, we finally obtain the local approximation

$$\hat{\mathcal{K}}(\eta_2) := \frac{1}{4\xi^2} \frac{1}{c_2\eta_2^2 + c_1\eta_2 + c_0} \quad (32)$$

231 where the coefficients $c_0 = S^2(1 + 2\xi\alpha\mathcal{C})$, $c_1 = \frac{1}{2}\xi(1 + (1 - 4\alpha)(1 - 2S^2))$ and $c_2 = 1 + 2\xi(1 - \alpha)\mathcal{C}$ are truncated
 232 to their first order terms in their respective Mac Laurin series expansion for ξ . This approximation is a little
 233 bit more complicated than (26) but has a somewhat similar format. However, as $\alpha \rightarrow 1$, i.e. $\mathcal{C} \rightarrow 0$ and $S \rightarrow 1$,
 234 coefficients c_0 , c_1 and c_2 respectively tend to 1, 2ξ and 1 which is slightly different from the coefficients 1, $-2\mathcal{C}$
 235 and 1 in $\hat{\mathcal{K}}(\eta_1)$. This difference should be manageable as long as both ξ and \mathcal{C} remain small (compared to one);
 236 it also highlights the limitations of the first approximation.

237 Figure 6 shows $\mathcal{K}(\eta_2)$ and $\hat{\mathcal{K}}(\eta_2)$. As expected, with this second stretching, the peaks in the stretched
 238 coordinate system are almost centered on $\eta_2 = 0$ no matter the value of the fractional exponent α , while the
 239 first stretching provides peaks centered on $\eta_1 = 0$ only as $\alpha \rightarrow 1$. Also, the integrand and the local approximation
 240 are virtually superimposed in the range $[-4, 4]$, which announces an accurate result.

241 Assuming again that the power spectral density of the loading does not significantly vary in the neighborhood
 242 of $\Omega = \Omega_p$, the corresponding approximation of the remainder is

$$\hat{r}_1 = S_u (1 + \mathcal{C}\xi) \int_{-\infty}^{+\infty} \hat{\mathcal{K}}(\eta_2) \xi d\eta_2 = \frac{S_u (1 + \mathcal{C}\xi)}{4\xi^2} \xi \left[\frac{2}{\rho} \arctan \frac{c_1 + 2c_2\eta}{\rho} \right]_{-\infty}^{+\infty} = \frac{\pi S_u (1 + \mathcal{C}\xi)}{2\rho\xi} \quad (33)$$

243 where $\rho = \sqrt{4c_0c_2 - c_1^2} = [4(1 + 2\xi\mathcal{C})\mathcal{S}^2 + \text{ord}(\xi^2)]^{1/2}$. Truncating again ρ to its leading order terms, and
 244 multiplying \hat{r}_1 by 2 to take both peaks into account, the resonant contribution to the response finally reads

$$\sigma_{x,r}^2 = \frac{\pi S_u (1 + \mathcal{C}\xi)}{2\mathcal{S}\xi\sqrt{1 + 2\xi\mathcal{C}}}. \quad (34)$$

245 This approximation is slightly richer than (29) in the sense that (29) was not designed for α different from
 246 1 (i.e. \mathcal{C} different from 0), while (34) was designed to provide an approximation in the more general case.
 247 Because (34) is not much more complicated than (29), it is naturally recommended to use (34) and consider
 248 $\tilde{\sigma}_{x,r}^2$ as a (simpler) variant of the resonant contribution. The only major difference is that the algebra required
 249 to establish (34) was a bit more involved.

250 4.3. Summary

251 To summarize, the background/resonant decomposition of the variance of a linear oscillator with fractional
 252 derivatives is given by

$$\sigma_x^2 = \sigma_{x,b}^2 + \sigma_{x,r}^2 = \int_{-\infty}^{+\infty} \frac{S_u(\Omega)}{1 + 4\xi\mathcal{C}|\Omega|^\alpha + 4\xi^2|\Omega|^{2\alpha}} d\Omega + \frac{\pi S_u (1 + \mathcal{C}\xi)}{2\mathcal{S}\xi\sqrt{1 + 2\xi\mathcal{C}}}. \quad (35)$$

253 We have also derived two variants, one for the background and one for the resonant components. The variant
 254 for the background, $\tilde{\sigma}_{x,b}^2 = 1$, although a little less accurate than $\sigma_{x,b}^2$ might prove interesting since it avoids the
 255 computation of the fractional low passed energy of the loading $u(t)$. The variant for the resonant component
 256 $\tilde{\sigma}_{x,r}^2$ is not much simpler but was obtained with a simpler derivation. It is not really worth being considered in
 257 practical applications.

258 Substituting back with the original variables of the problem

$$\sigma_y^2 = \frac{1}{k^2} \int_{-\infty}^{+\infty} \frac{S_f(\omega_0) d\omega}{1 + 4\xi\mathcal{C} \left| \frac{\omega}{\omega_0} \right|^\alpha + 4\xi^2 \left| \frac{\omega}{\omega_0} \right|^{2\alpha}} + \frac{1}{k^2} \frac{\pi\omega_0 S_f[\omega_0(1 + \mathcal{C}\xi)]}{2\mathcal{S}\xi\sqrt{1 + 2\xi\mathcal{C}}} \quad (36)$$

259 where $\omega_0 = 1/t^* = \sqrt{k/m}$ is the natural circular frequency of the undamped system.

260 5. Validation, illustrations and discussion

261 The accuracy of the proposed formulation will be assessed by comparison with the exact result. The exact
 262 result is obtained by numerical integration of the exact power spectral density of the response. Integration
 263 is performed with the adaptive algorithm proposed in Wolfram Mathematica [24], with default integration
 264 parameters of Version 11.0.1.0.

265 5.1. Validation: white noise excitation

266 As a validation case, the response of an oscillator equipped with a viscoelastic device and subjected to a
 267 delta correlated excitation is considered. This problem has already been tackled with a stochastic averaging
 268 approach, e.g. [46]. Both the stochastic averaging and the multiple timescale spectral analysis are based on
 269 the same assumption that the damping ratio (or fractional coefficient ξ) is a small parameter. To compare
 270 them both therefore borders more on the confrontation than validation, which is considered in a second step by
 271 comparison with the exact solution.

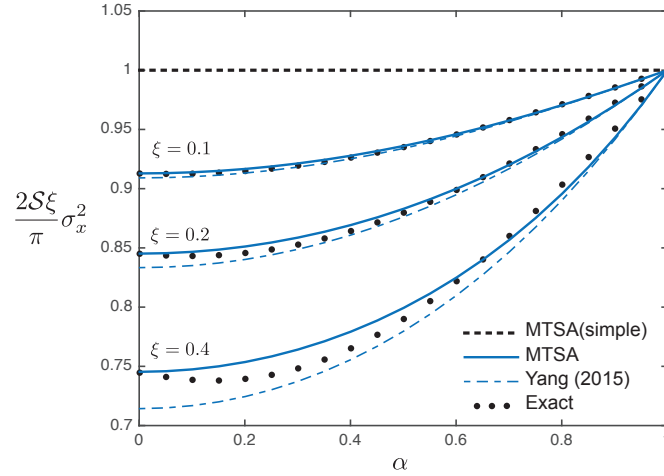


Figure 7: Variance of the response of a fractional oscillator subjected to a unit white noise excitation. (Please see online version for colors)

272 In the multiple timescale spectral analysis (MTSA) formulation, the background component needs to be
 273 discarded, since the variance of the delta-correlated noise is infinite. We are therefore left with the resonant
 274 component $\sigma_{x,r}^2$ (or $\tilde{\sigma}_{x,r}^2$) where $S_u(1 + \mathcal{C}\xi)$ is replaced by 1, which yields

$$\frac{2\mathcal{S}\xi}{\pi}\sigma_x^2 = \frac{1}{\sqrt{1 + \xi\mathcal{C}}} \quad \text{or} \quad \frac{2\mathcal{S}\xi}{\pi}\tilde{\sigma}_x^2 = 1, \quad (37)$$

275 while the approximation derived in [46] reads, with our notations,

$$\frac{2\mathcal{S}\xi}{\pi}\sigma_x^2 = \frac{1}{1 + \xi\mathcal{C}}. \quad (38)$$

276 First, we recognize that all three approximations have the same leading order behaviors in ξ and α , which are
 277 expressed by the leading product $\mathcal{S}\xi$, repelled to the lefthand side. The slight differences on the righthand
 278 side are therefore associated with the second order terms. This is a first validation of the appropriateness of
 279 the solutions we have developed, since it recovers the same leading order solution as the reputed stochastic
 280 averaging response. Figure 7 shows these three results (the righthand side) and provides a comparison with
 281 the exact result, represented with back dots. In all cases, the simple MTSA formulation fails to finely capture
 282 the second-order dependency in α . For $\xi = 0.1$, both the MTSA and the stochastic averaging (Yang 2015)
 283 formulations are almost perfect. For larger fractional coefficients, $\xi = 0.2$ and $\xi = 0.4$, these two solutions
 284 capture the right trend but are naturally much less accurate, since they are developed under the assumption
 285 $\xi \ll 1$. However the multiple timescale spectral analysis method recovers the exact result in the limit case
 286 $\alpha = 0$, while the stochastic averaging is consistently underestimating the exact result.

287 5.2. Illustration: buffeting type excitation

288 The governing equation (6) is now considered together with the buffeting loading described by (8). Figures
 289 8 and 9 show the variance of the response obtained with the proposed formulation (MTSA) and by numerical
 290 integration of the exact analytical formulation. The variance is represented as a function of α for given values
 291 of ξ , and as a function of ξ for given values of α . In both figures, the background component $\sigma_{x,b}^2$ is shown with
 292 dashed lines. This is to illustrate two facts: (i) the smaller ξ and the larger α , the better the approximation
 293 $\tilde{\sigma}_{x,b}^2 = 1$; this approximation seems reasonable for $\xi \lesssim 10^{-2}$ (ii) the behavior of the system is quasi-static for
 294 large ξ or large α , since the total variance (MTSA) is very close to the background component in those areas.

295 For $\beta = 0.01$ (on the left), the proposed approximation provides a very accurate estimation of the variance
 296 of the response, throughout the different scales of ξ and over the whole range $[0, 1]$ for α . Figure 10 represents
 297 the relative error realized with the proposed approximation and indeed confirms that the error remains smaller
 298 than 1% for $\xi < 10^{-2}$, no matter the value of α . The contours of the error curve up for small values of α which
 299 is, again, a consequence of the accuracy of the resonant component (the only one that matters as $\alpha \rightarrow 0$) in this
 300 limit case. The central plot in Figure 10 shows the relative error obtained with the approximation $\tilde{\sigma}_{x,b}^2 + \sigma_{x,r}^2$,
 301 i.e. by changing the way the background contribution is computed. As expected, for $\xi \lesssim 10^{-2}$, the response is
 302 mostly resonant and the error is not affected by the way the background component is estimated. For $\xi > 10^{-2}$,
 303 the response is mostly quasi-static and the background component is more important. In that case, the error

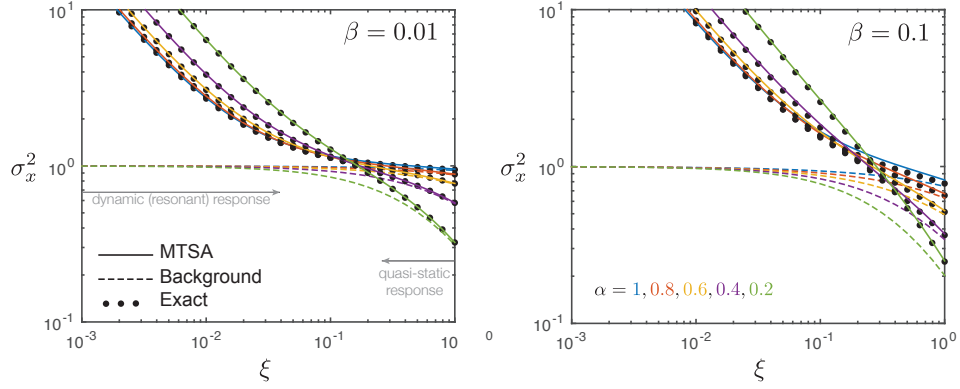


Figure 8: Variances of the response of the system subjected to the buffeting type excitation, for $\beta = 0.01$ (left) and $\beta = 0.1$ (right). Represented as a function of the fractional coefficient ξ and for various values of the fractional exponent α . (Please see online version for colors)

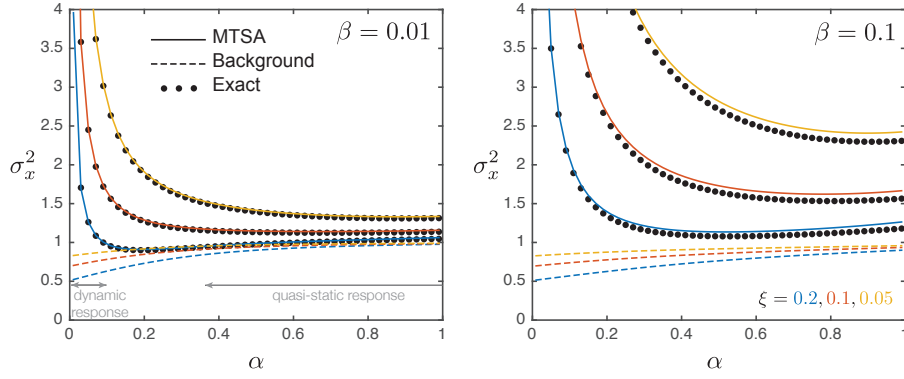


Figure 9: Variances of the response of the system subjected to the buffeting type excitation, for $\beta = 0.01$ (left) and $\beta = 0.1$ (right). Represented as a function of the fractional exponent α and for various values of the fractional coefficient ξ . (Please see online version for colors)

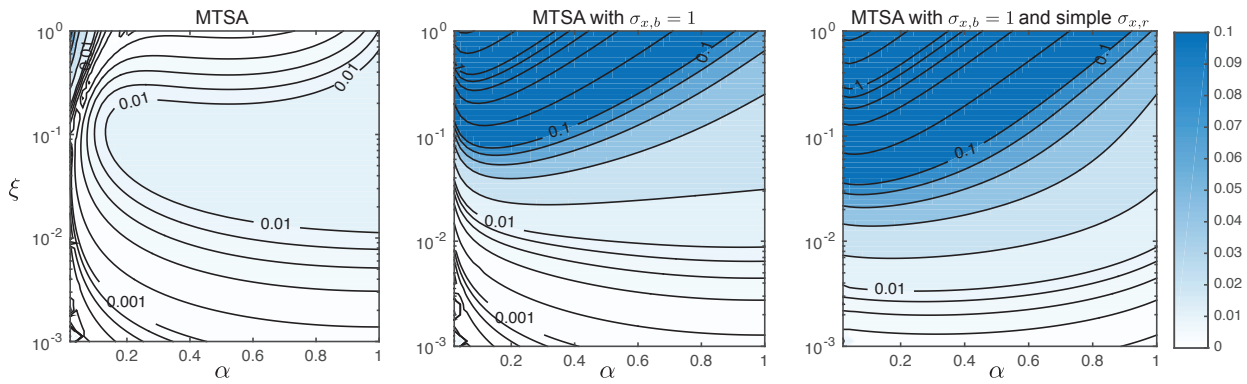


Figure 10: Relative error on the variance of the response of a fractional oscillator subjected to a low frequency turbulent loading, as a function of the fractional exponent α and the fractional coefficient ξ . (Please see online version for colors)

grows slightly more proportionally than ξ . On the right, Figure 10 shows the relative error obtained with the approximation $\tilde{\sigma}_{x,b}^2 + \tilde{\sigma}_{x,r}^2$. In that case, both the background and the resonant components are too roughly estimated. This results in errors of a few percents as soon as $\xi > 5 \cdot 10^{-3}$.

6. Conclusions

In this paper, we have applied the multiple timescale spectral analysis to the structural analysis of a linear system equipped with a viscoelastic device. Compared to the well-known solution of the linear viscous problem, it has been shown that the background component requires a little more attention, especially as soon as the fractional coefficient ξ is larger than or similar to 10^{-2} . In that case, a lowpass fractional filter of the excitation needs to be considered to establish the background component. The resonant component of the response is also affected by the presence of the viscoelastic device. At first order, it is simply obtained by dividing the classical response in the viscous case by $\mathcal{S} = \sin \frac{\alpha\pi}{2}$. Several solutions have been proposed and discussed. Among them, (35-36) should be preferred.

The game of stretching and rescaling that rules the multiple timescale spectral analysis offers more flexibility to derive approximate solutions than standard time-domain methods. The resulting approximation might not necessarily be optimal, in one (or some) sense, but at least may features interesting advantages. For instance, the proposed solution is shown to provide more accurate results than those obtained with the stochastic averaging method, as the fractional exponent $\alpha \rightarrow 0$.

Extrapolating on these promising results, further works should extend to slightly nonlinear or multiple degree-of-freedom structures.

References

- [1] Jun-Feng A Zhao. Stochastic response of dynamical systems with fractional derivative term under wide-band excitation. *Mathematical Problems in Engineering*, page 9, 2016.
- [2] O.P. Agrawal. Stochastic analysis of dynamic systems containing fractional derivatives. *Journal of Sound and Vibration*, 247(5):927 – 938, 2001.
- [3] Gioacchino Alotta, Giuseppe Failla, and Massimiliano Zingales. Finite-element formulation of a nonlocal hereditary fractional-order timoshenko beam. *Journal of Engineering Mechanics*, 143(5):D4015001, 2017.
- [4] R L Bagley and P J Torvik. Fractional calculus in the transient analysis of viscoelastically damped structures. *AIAA Journal*, 23(6):918–925, jun 1985.
- [5] T. Canor, N. Blaise, and V. Denoël. Efficient uncoupled stochastic analysis with non-proportional damping. *Journal of Sound and Vibration*, 331(24):5283 – 5291, 2012.
- [6] Thomas Canor, Luca Caracoglia, and Vincent Denoël. Perturbation methods in evolutionary spectral analysis for linear dynamics and equivalent statistical linearization. *Probabilistic Engineering Mechanics*, 46:1 – 17, 2016.
- [7] L.C. Chen, Q.Q. Zhuang, and W.Q. Zhu. Response of s dof nonlinear oscillators with lightly fractional derivative damping under real noise excitations. *The European Physical Journal Special Topics*, 193(1):81–92, Mar 2011.
- [8] Lincong Chen, Fang Hu, and Weiqiu Zhu. Stochastic dynamics and fractional optimal control of quasi integrable hamiltonian systems with fractional derivative damping. *Fractional Calculus and Applied Analysis*, 16(1):189–225, Mar 2013.
- [9] Lincong Chen, Weihua Wang, Zhongshen Li, and Weiqiu Zhu. Stationary response of duffing oscillator with hardening stiffness and fractional derivative. *International Journal of Non-Linear Mechanics*, 48:44 – 50, 2013.
- [10] Lincong Chen, Qingqu Zhuang, and Weiqiu Zhu. First passage failure of mdof quasi-integrable hamiltonian systems with fractional derivative damping. *Acta Mechanica*, 222(3):245–260, Dec 2011.
- [11] Natalia Colinas-Armijo and Mario Di Paola. Step-by-step integration for fractional operators. *Communications in Nonlinear Science and Numerical Simulation*, 59:292 – 305, 2018.
- [12] Giulio Cottone and Mario Di Paola. Fractional spectral moments for digital simulation of multivariate wind velocity fields. *Journal of Wind Engineering and Industrial Aerodynamics*, 99(6):741 – 747, 2011. The Eleventh Italian National Conference on Wind Engineering, IN-VENTO-2010, Spoleto, Italy, June 30th - July 3rd 2010.
- [13] V Denoël. Estimation of modal correlation coefficients from background and resonant responses. *Structural Engineering and Mechanics: an International Journal*, 32(6):725–740, 2009.
- [14] V Denoël. On the background and biresonant components of the random response of single degree-of-freedom systems under non-Gaussian random loading. *Engineering Structures*, 33(8):2271–2283, 2011.
- [15] V Denoël. Multiple timescale spectral analysis. *Probabilistic Engineering Mechanics*, 39(0):69–86, jan 2015.
- [16] Vincent Denoël and Luigi Carassale. Response of an oscillator to a random quadratic velocity-feedback loading. *Journal of Wind Engineering and Industrial Aerodynamics*, 147:330 – 344, 2015.
- [17] Mario Di Paola, Antonina Pirrotta, Francesco Paolo Pinnola, and Salvatore Di Lorenzo. Stochastic response of fractionally damped beams. *PROBABILISTIC ENGINEERING MECHANICS*, 35:37–43, 2014.
- [18] Mikael Enelund and B Lennart Josefson. Time-Domain Finite Element Analysis of Viscoelastic Structures with Fractional Derivatives Constitutive Relations. *AIAA Journal*, 35(10):1630–1637, oct 1997.
- [19] Giuseppe Failla. Stationary response of beams and frames with fractional dampers through exact frequency response functions. *Journal of Engineering Mechanics*, 143(5):D4016004, 2017.
- [20] Mircea Grigoriu. Linear systems with fractional brownian motion and gaussian noise. *Probabilistic Engineering Mechanics*, 22(3):276 – 284, 2007.
- [21] E J Hinch. *Perturbation Methods*, volume 1. Cambridge University Press, Cambridge, 1991.
- [22] Yaozhong Hu and Bernt Oksendal. Fractional white noise calculus and applications to finance. *Infinite Dimensional Analysis, Quantum Probability and Related Topics*, 06(01):1–32, 2003.

- 367 [23] Z. L. Huang, X. L. Jin, C. W. Lim, and Y. Wang. Statistical analysis for stochastic systems including fractional derivatives.
368 *Nonlinear Dynamics*, 59(1):339–349, Jan 2010.
- 369 [24] Wolfram Research, Inc. Mathematica, Version 11.0. Champaign, IL, 2016.
- 370 [25] C. Ionescu, A. Lopes, D. Copot, J. A. T. Machado, and J. H. T. Bates. The role of fractional calculus in modeling biological
371 phenomena: A review. *Communications in Nonlinear Science and Numerical Simulations*, 51:141–159, October 2017.
- 372 [26] Guy Jumarie. Path integral for the probability of the trajectories generated by fractional dynamics subject to gaussian white
373 noise. *Applied Mathematics Letters*, 20(8):846 – 852, 2007.
- 374 [27] Ioannis A Kougioumtzoglou, Alberto Di Matteo, Pol D Spanos, Antonina Pirrotta, and Mario Di Paola. An Efficient Wiener
375 Path Integral Technique Formulation for Stochastic Response Determination of Nonlinear MDOF Systems. *Journal of Applied
376 Mechanics*, 82(10):101005–101007, jul 2015.
- 377 [28] Ioannis A. Kougioumtzoglou and Pol D. Spanos. Harmonic wavelets based response evolutionary power spectrum determination
378 of linear and non-linear oscillators with fractional derivative elements. *International Journal of Non-Linear Mechanics*, 80:66
379 – 75, 2016. Dynamics, Stability, and Control of Flexible Structures.
- 380 [29] Ye Kun, Li Li, and Tang Jiaxiang. Stochastic seismic response of structures with added viscoelastic dampers modeled by
381 fractional derivative. *Earthquake Engineering and Engineering Vibration*, 2(1):133–139, Jun 2003.
- 382 [30] A. Lotfi and S.A. Yousefi. A numerical technique for solving a class of fractional variational problems. *Journal of Computational
383 and Applied Mathematics*, 237(1):633 – 643, 2013.
- 384 [31] R.L. Magin. *Fractional Calculus in Bioengineering*. Begell House Publishers, 2006.
- 385 [32] Nicos Makris and M. C. Constantinou. Fractional-derivative maxwell model for viscous dampers. *Journal of Structural
386 Engineering*, 117(9):2708–2724, 1991.
- 387 [33] Alberto Di Matteo, Ioannis A. Kougioumtzoglou, Antonina Pirrotta, Pol D. Spanos, and Mario Di Paola. Stochastic response
388 determination of nonlinear oscillators with fractional derivatives elements via the wiener path integral. *Probabilistic Engineering
389 Mechanics*, 38:127 – 135, 2014.
- 390 [34] A. Palmeri, F. Ricciardelli, G. Muscolino, and A. De Luca. Random vibration of systems with viscoelastic memory. *Journal
391 of Engineering Mechanics*, 130(9):1052–1061, 2004.
- 392 [35] Mario Di Paola, Giuseppe Failla, and Antonina Pirrotta. Stationary and non-stationary stochastic response of linear fractional
393 viscoelastic systems. *Probabilistic Engineering Mechanics*, 28:85 – 90, 2012.
- 394 [36] A Preumont. *Random Vibration and Spectral Analysis*. Kluwer Academic Publishers, 1994.
- 395 [37] E Simiu and R Scanlan. *Wind Effects On Structures*. John Wiley and Sons, New-York, 3rd edition, 1996.
- 396 [38] G Solari and G Piccardo. Probabilistic 3-D turbulence modeling for gust buffeting of structures. *Probabilistic Engineering
397 Mechanics*, 16(1):73–86, 2001.
- 398 [39] P. D. Spanos and B. A. Zeldin. Random vibration of systems with frequency-dependent parameters or fractional derivatives.
399 *Journal of Engineering Mechanics*, 123(3):290–292, 1997.
- 400 [40] Pol D. Spanos and Georgios I. Evangelatos. Response of a non-linear system with restoring forces governed by fractional deriva-
401 tives: Time domain simulation and statistical linearization solution. *Soil Dynamics and Earthquake Engineering*, 30(9):811 –
402 821, 2010.
- 403 [41] Wei Sun, Zhuo Wang, Xianfei Yan, and Mingwei Zhu. Inverse identification of the frequency-dependent mechanical parameters
404 of viscoelastic materials based on the measured frfs. *Mechanical Systems and Signal Processing*, 98:816 – 833, 2018.
- 405 [42] V. Valimaki and T. I. Laakso. Principles of fractional delay filters. In *2000 IEEE International Conference on Acoustics,
406 Speech, and Signal Processing. Proceedings (Cat. No.00CH37100)*, volume 6, pages 3870–3873 vol.6, 2000.
- 407 [43] H. Vanvinckenroye and V. Denoël. Average first-passage time of a quasi-hamiltonian mathieu oscillator with parametric and
408 forcing excitations. *Journal of Sound and Vibration*, 406:328 – 345, 2017.
- 409 [44] Yong Xu, Yongge Li, and Di Liu. Response of Fractional Oscillators With Viscoelastic Term Under Random Excitation.
410 *Journal of Computational and Nonlinear Dynamics*, 9(3):31015–31018, feb 2014.
- 411 [45] Yongge Yang, Wei Xu, Xudong Gu, and Yahui Sun. Stochastic response of a class of self-excited systems with caputo-type
412 fractional derivative driven by gaussian white noise. *Chaos, Solitons and Fractals*, 77:190 – 204, 2015.
- 413 [46] Yongge Yang, Wei Xu, Wantao Jia, and Qun Han. Stationary response of nonlinear system with caputo-type fractional
414 derivative damping under gaussian white noise excitation. *Nonlinear Dynamics*, 79(1):139–146, Jan 2015.

415